Robotica (2019) volume 37, pp. 1225–1239. © Cambridge University Press 2018
doi:10.1017/S0263574718000711

Parametric dynamic analysis of walking within a cable-based gait trainer

Houssein Lamine†,* Lotfi Romdhane†, ‡, and Sami Bennour†

†*Mechanical Laboratory of Sousse (LMS), National Engineering School of Sousse, University of Sousse, Sousse 4000, Tunisia*
‡*Mechanical Engineering Department, American University of Sharjah, PO Box 26666, Sharjah, United Arab Emirates*
E-mail: lotfi.romdhane@gmail.com, sami.bennour@gmail.com

(Accepted July 18, 2018)

SUMMARY
In this paper, a parametric analysis of the inverse dynamics of an upright partially unloaded walking is performed. This motion is produced through a gait-training machine emulating the over-ground walking using a body weight support mechanism and a cable-driven robot. The input motion is the kinematics of a normal gait, and the ultimate output result is the required tensions to be generated by the cable robot in order to drive the lower limb. The dynamic analysis is carried out based on the Newton–Euler approach. A Matlab Simscape model is also built to validate the analytical results. The obtained dynamic model is used to investigate the effect of the variation of the gait simulation parameters on the actuation wrench and the cable tensions. The obtained results could be used to determine the optimal design of the gait trainer actuators and they are useful in estimating optimal gait training parameters.

KEYWORDS: gait analysis, cable-driven robots, gait training, partial unloaded walking, Newton–Euler, Matlab Simscape

1. Introduction

The Human gait analysis has been widely investigated in various applications: identification of gait pathologies, fall risk, evaluation of neurological diseases and rehabilitation progress, therapy design for impaired subjects, design of orthoses and prosthetics.[1–5] Generally speaking, gait analysis includes two parts: motion analysis and motion simulation. The first one consists of acquiring quantitative kinematic and dynamic data. These data can be post-processed to yield information about the gait of a patient. The motion simulation requires a biomechanical model of the lower limb, which allows the simulation of the movement of interest.[6,7] These movements are, usually, activities of daily living such as walking, running, climbing and jumping.[8]

One of the most common systems for motion tracking is based on a set of cameras and reflective skin markers. The cameras simultaneously film the marker, which allows the tracking of its position during the motion. Other motion capture devices can be used such as 3D depth cameras (e.g., Kinect[10]), inertial measurement units (accelerometer and gyroscope), goniometers and tapes, markless camera-based systems and electromagnetic tracking systems.[11] In some cases, a force plate is used to record the ground reaction force (GRF) during the motion.[9] In-sole pressure measurement sensors or pressure mats[12] could also be used as an alternative to force plates. Electromyography (EMG) is also used to access the muscle activities, which can give an estimate of the GRF. These kinematic and dynamic measurements are used to validate the complex models required to describe the kinematic and dynamics of the lower limb.[13,8] Some of these models address only the skeletal

* Corresponding author. E-mail: houssein.lamine@gmail.com

system,[7] whereas others, more complex, address the musculoskeletal system to include the muscles' forces in the dynamic model.[3] Some authors propose to include the control system, which leads to a neuromusculoskeletal model.[5]

In this paper, the design of a gait training machine called the cable-driven legs trainer (CDLT)[14] is proposed. Such a device is used for the rehabilitation of patients having a gait disorders. In general, for neurological deficits (SCI or Stroke) where motor/sensory functions are partially preserved, intense and task-specific practice of the gait stepping motion allows the recovery of independent over-ground walking.[15] The use of cable robots in gait rehabilitation is motivated due to their versatility and their low cost. Indeed, the same mechanical design can be easily adapted to rehabilitate small children or tall elder person. Furthermore, modifying the structure, e.g., adding or removing cables, allows the user to easily modify the degree of freedom (DOF) of the system to adapt it to his need.

The first task in this work is to perform an inverse dynamic simulation of a gait using the CDLT. The human body is modeled as a planar multi-segment mechanism. Furthermore, inertia and length specifications of each segment are obtained from anthropometry.[6,16] The estimation or prediction of the GRF has been widely investigated in the literature.[9,17–21] In this work, the approach presented in refs. [6] and [13] will be used; the measured kinematics parameters and the GRFs are used as input data for the human body model in order to estimate the required actuation wrench. The HuMoD open database is post-processed for this purpose, i.e., to get the kinematic and dynamic data.[8] Moreover, one fundamental issue is to solve the double stance redundant problem.[21] In such a case, the upper body load is divided between the two feet. Several approaches have been investigated to solve this issue such as the shift function,[17] the smooth transition assumption[18] and the detailed contact model.[21] In our case, based on the measured vertical GRFs of the right and left feet, a shift coefficient is computed in order to define the amount of force for each limb. The obtained dynamic model is simulated using two methods: Newton–Euler (N–E) approach[22] and Matlab Simscape. Further, two simulation scenarios are presented: on-ground walking and off-ground walking.

The paper is organized as follows: In Section 2, a dynamic model of the human body is presented. Then, the free-body diagram and the dynamic equations are given in Section 3. A dynamic simulation using Matlab Simscape is investigated in Section 4. Computation of the cable tensions is given in Section 5. In the last section, the effects of changes in gait simulation parameters on the actuation wrench and the cable tensions are discussed.

2. Dynamic Modeling

The CDLT is a cable robot-based gait training machine shown in Fig. 1. It includes

(a) a passive elastic body weight support device (BWSD)[23] to suspend the patient in a vertical posture while applying a certain amount of unloading,
(b) a cable-driven leg manipulator (CDLM) to move the lower limb in the sagittal plane through the leg's orthosis (O), which is controlled by four cables and
(c) a treadmill (T) to allow the forward movement of walking. For a detailed description of the CDLT, the reader is referred to ref. [14].

As depicted in Fig. 2(a), the body is represented by a planar four-link mechanism, representing the upper body (known also as HAT segment[13]), the thigh, the leg and the foot. The joint between the trunk and the fixed frame is modeled as a prismatic joint. For the hip, the knee and the ankle, they are modeled as revolute joints.

Based on anthropometry,[6] the geometry of the lower limb is written as a function of the body height h (Fig. 2(b)). C_1, C_2 and C_3 are the centers of mass (CoM) of the thigh, the leg and the foot, respectively. Furthermore, H, K and A are joint centers of the hip, the knee and the ankle, respectively. All points are defined in relation to their local coordinate systems and the global reference frame is $O, \boldsymbol{x}_0, \boldsymbol{y}_0$. The mass and moment of inertia of each segment are also determined as a function of the body mass m and/or height h (Fig. 2(d)).

It is important to mention that the following assumptions were made:

- All the joints are considered passive and frictionless;[13] thus, there are no transmitted torques.
- There is no relative motion between the orthosis and the leg.

https://doi.org/10.1017/S0263574718000711 Published online by Cambridge University Press

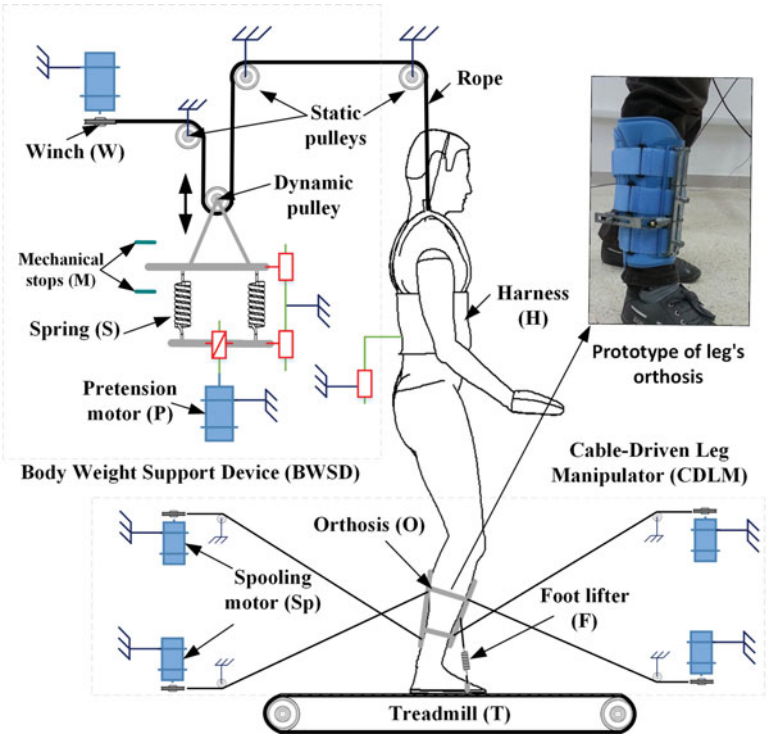

Fig. 1. Diagram of the cable-driven legs trainer (CDLT).

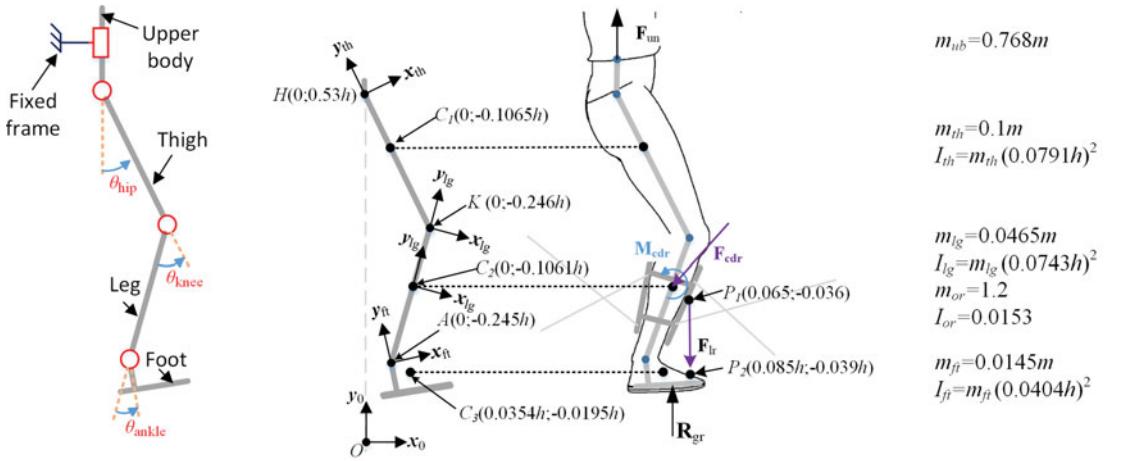

Fig. 2. Dynamic modeling of the human body (SI unit).

- The lower limb kinematics is the same as during a normal walking. Furthermore, even when the ankle joint is not actuated, the same general trajectory is observed.[24]

The main external loads acting on the human body are (Fig. 2(c)) as follows:

- $\mathbf{F}_{un}$, the unloading force produced by the BWSD,
- $\mathbf{R}_{gr}$, the GRF applied at the sole of the foot,
- $\mathbf{F}_{lr}$, the footlifter force acting between the leg's orthosis and the foot which can be neglected,
- $\mathbf{F}_{cdr}$ and $\mathbf{M}_{cdr}$, the resultant wrench, which is the actuation unknowns of the inverse dynamic simulation.

https://doi.org/10.1017/S0263574718000711 Published online by Cambridge University Press

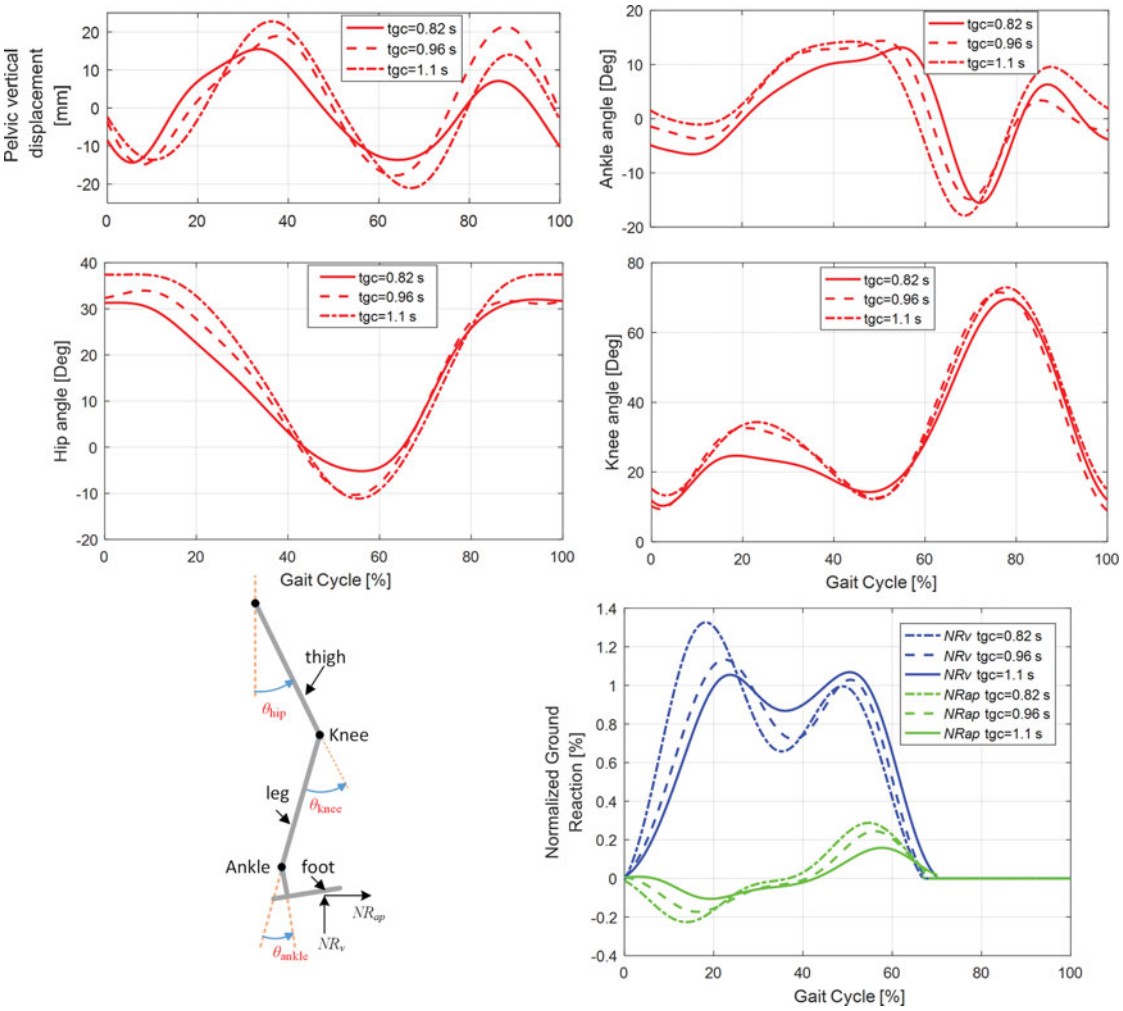

Fig. 3. Gait kinematics and dynamics.

The desired performance or the input information of the inverse dynamic simulation is the kinematics of a recorded normal gait, whereas the output result is the required actuation wrench applied through the leg orthosis.

In order to get the gait kinematics and dynamics for different speeds, the HuMoD open database[8] is employed. The curve representing the straight walking data, as a function of time, for a male subject is smoothed using a fifth-order Butterworth filter. Figure 3 depicts joint trajectories of the pelvis, the hip, the knee and the ankle, and further, the vertical (NR_v) and the anterior–posterior (NR_{ap}) GRFs. The three different walking speeds correspond to times of gait cycle (tgc) of 1.1 s, 0.96 s and 0.82 s, respectively.

It is worth mentioning that for gait training, two scenarios have to be considered: the off-ground walking and the on-ground walking. The first happens at the beginning of a training session when some cycles of an off-ground walking are achieved for familiarization. The sole of the foot is 0.1 m above the treadmill when the lower limb lies vertically. Then, the on-ground walking takes place.

3. Newton–Euler Approach

The following description is carried out with the involvement of one limb. The free-body diagram of the human body is shown in Fig. 4. It depicts all applied forces on the upper body, the thigh, the leg and the foot. The main external and inter-segmental forces are as follows: the unloading force $\mathbf{F}_{un,}$ the upper body force $\mathbf{F}_{ub}$, the thigh force $\mathbf{F}_{th}$, the foot force $\mathbf{F}_{ft}$ and the GRF $\mathbf{R}_{gr}$.

https://doi.org/10.1017/S0263574718000711 Published online by Cambridge University Press

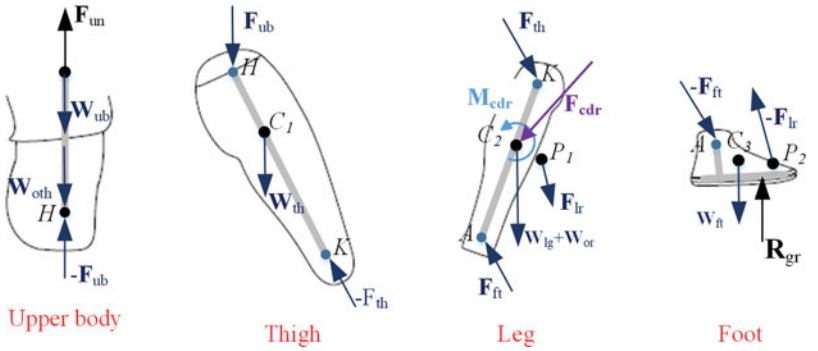

Fig. 4. Free-body diagrams of body segments.

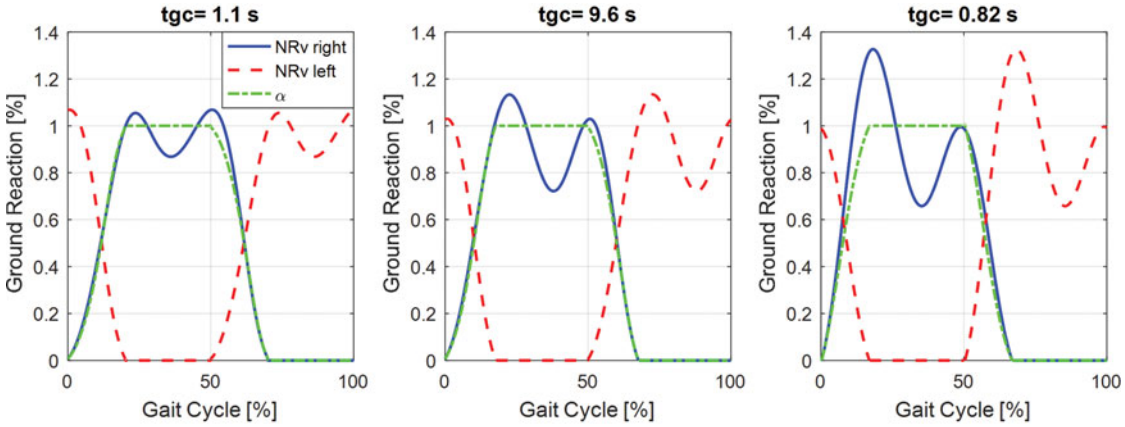

Fig. 5. Curve of α coefficient.

One shall note that the equilibrium equations are written at the CoM of each segment; thus, moments of the gravity forces are zero. Furthermore, the transmitted torque from one segment to another, around the axis of the joint, is taken as zero, since the joints are assumed to be passive. The investigated N–E equations are solved recursively in order to get the actuation wrench. In the following, the dynamic analysis is given for one lower limb; however, the effect of the opposite limb is taken into account.

During the walking phase, the upper body is assumed to be translating along the vertical direction. The equilibrium of the upper body can be written as follows:

$$\mathbf{F}_{\text{un}} - (1/\alpha) \cdot \mathbf{F}_{\text{ub}} + \mathbf{W}_{\text{ub}} + \mathbf{W}_{\text{oth}} = (m_{\text{ub}} + m_{\text{th}}) \cdot \mathbf{a}_{\text{ub}} \tag{1}$$

where $\mathbf{F}_{\text{un}}$ is the unloading force, $\mathbf{W}_{\text{ub}}$ is the weight of the upper body, $\mathbf{F}_{\text{ub}}$ is the current thigh force, $\mathbf{W}_{\text{oth}}$ is the weight of the opposite thigh and $\mathbf{a}_{\text{ub}}$ is the upper body acceleration.

The opposite leg and foot are assumed to be balanced by the opposite orthosis; thus, in Eq. (1), only the thigh mass m_{ub} is considered. In addition, the unloading force $\mathbf{F}_{\text{un}}$, applied by the suspension system on the upper body through the harness, is given as follows:

$$\mathbf{F}_{\text{uny}} = (k/2) \cdot (y_0 + \Delta y/2) \text{ such that } y_0 = (\text{BWS} \cdot g \cdot m)/(k/2) \tag{2}$$

where k = 4 N/m is the total springs constant, $g = 9.81$ m/s^2 is the gravity acceleration, m is the body mass and Δy is the pelvic displacement (see Fig. 3). The springs offset y_0 is calculated based on the desired amount of unloading BWS; therefore, the spring pre-tension force is the mean value of the unloading force.

The term $(1/\alpha) \cdot F_{\text{ub}}$ represents the force transmitted from the HAT segment to the current thigh. α is a shift coefficient that defines the support of body weight of one limb [17]. α is equal to 1 during single limb stance and zero during swing time. During the walking, α varies from 0 to 1, based on the ratio between left and right vertical reactions of the feet:$\alpha = (NR_{v_{\text{right}}} + NR_{v_{\text{left}}})/NR_{v_{\text{right}}}$. Figure 5

https://doi.org/10.1017/S0263574718000711 Published online by Cambridge University Press

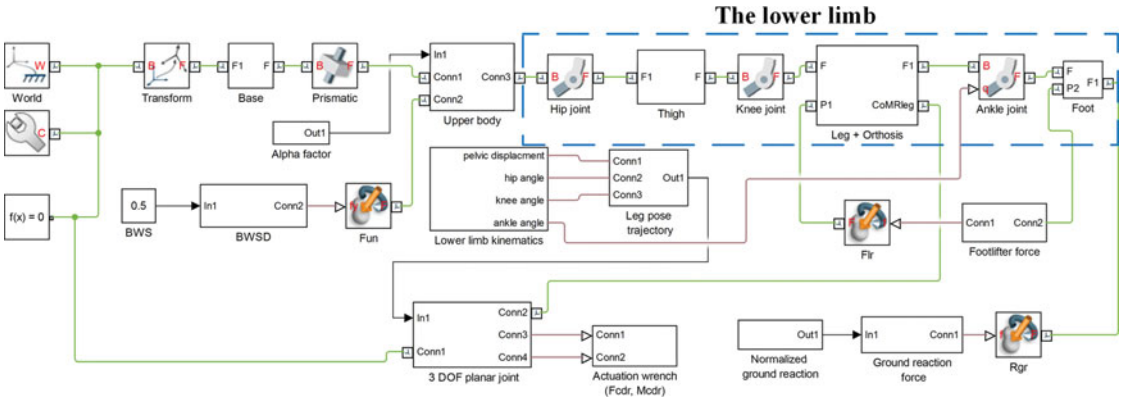

Fig. 6. Matlab Simscape model.

shows the change of this factor along with the variation of NR_v of the feet over one gait cycle for different gait cycle times.

Combining Eqs. (1) and (2) yields the upper body force $\mathbf{F}_{\text{ub}}$ for a given amount of unloading BWS. The details of the calculation are given in Appendix A.1.

The dynamic model of the thigh segment is given as follows:

$$\begin{aligned} \mathbf{F}_{\text{ub}} - \mathbf{F}_{\text{th}} + \mathbf{W}_{\text{th}} &= m_{\text{th}} \cdot \mathbf{a}_{\text{th}} \\ \mathbf{M}_{\text{ub}} - \mathbf{M}_{\text{th}} &= I_{\text{th}} \cdot \dot{\boldsymbol{\omega}}_{\text{th}} \end{aligned} \tag{3}$$

where $\mathbf{W}_{\text{th}}$, m_{th}, I_{th}, $\mathbf{a}_{\text{th}}$ and $\dot{\boldsymbol{\omega}}_{\text{th}}$ are the weight, the mass, the moment of inertia, the linear acceleration of the CoM and the angular acceleration of the thigh segment, respectively. The system of linear equations (3) is solved to obtain the expression of $\mathbf{F}_{\text{th}}$ (see Appendix A.2) exerted by the thigh on the leg.

Moving to the foot segment, the applied forces are as follows: the GRF $\mathbf{R}_{\text{gr}}$, the foot weight $\mathbf{W}_{\text{ft}}$, the thigh force $-\mathbf{F}_{\text{ft}}$ and the footlifter force $\mathbf{F}_{\text{lr}}$. The equilibrium of the foot can be written as follows:

$$\begin{aligned} -\mathbf{F}_{\text{ft}} - \mathbf{F}_{\text{lr}} + \mathbf{R}_{\text{gr}} + \mathbf{W}_{\text{ft}} &= m_{\text{ft}} \cdot \mathbf{a}_{\text{ft}} \\ -\mathbf{M}_{\text{ft}} - \mathbf{M}_{\text{lr}} + \mathbf{M}_{\text{gr}} &= I_{\text{ft}} \cdot \dot{\boldsymbol{\omega}}_{\text{ft}} \end{aligned} \tag{4}$$

where m_{ft}, I_{ft}, $\mathbf{a}_{\text{ft}}$ and $\dot{\boldsymbol{\omega}}_{\text{th}}$ are the mass, the moment of inertia, the linear acceleration of the CoM and the angular acceleration of the foot segment, respectively.

The ground force $\mathbf{R}_{\text{gr}}$ is calculated as follows:

$$\mathbf{R}_{\text{gr}} = W_n \cdot \mathbf{NR}_{\text{gr}} \text{ such that } W_n = (m + m_{\text{or}} - m_{\text{lg}} - m_{\text{ft}}) \cdot g - F_{\text{uny}} \text{ and } \mathbf{NR}_{\text{gr}} = \begin{pmatrix} NR_v & NR_{\text{ap}} \end{pmatrix}^T \tag{5}$$

Note that $\mathbf{F}_{\text{lr}}$ is only active during the swing phase and it is computed based on the moment equilibrium. Therefore, the solution of the foot force F_{ft} is given in Appendix A.3.

Considering the leg segment, its equilibrium, provided in Eq. (6), is marked by the terms of the actuation wrench $\mathbf{F}_{\text{cdr}}$ and $\mathbf{M}_{\text{cdr}}$. The evaluation of Eq. (6) allows to obtain the expression of the actuation wrench (see Appendix A.4):

$$\begin{aligned} \mathbf{F}_{\text{th}} + \mathbf{F}_{\text{ft}} + \mathbf{W}_{\text{lg}} + \mathbf{W}_{\text{or}} + \mathbf{F}_{\text{lr}} + \mathbf{F}_{\text{cdr}} &= (m_{\text{lg}} + m_{\text{or}}) \cdot \mathbf{a}_{\text{lg}} \\ \mathbf{M}_{\text{th}} + \mathbf{M}_{\text{ft}} + \mathbf{M}_{\text{lr}} + \mathbf{M}_{\text{cdr}} &= (I_{\text{lg}} + I_{\text{or}}) \cdot \dot{\boldsymbol{\omega}}_{\text{lg}} \end{aligned} \tag{6}$$

One shall note that, during gait simulation, linear and angular accelerations are obtained through numerical differentiation of the pose equations of body segments (see Appendices A.5, A.6 and A.7) using the kinematics of a normal gait (see Fig. 5(a)).

4. Matlab Simscape Model

In this section, we present the Matlab Simscape model of the lower limb. The first step in model development is the creation of body parts and the definition of joints. The developed Simscape model

https://doi.org/10.1017/S0263574718000711 Published online by Cambridge University Press

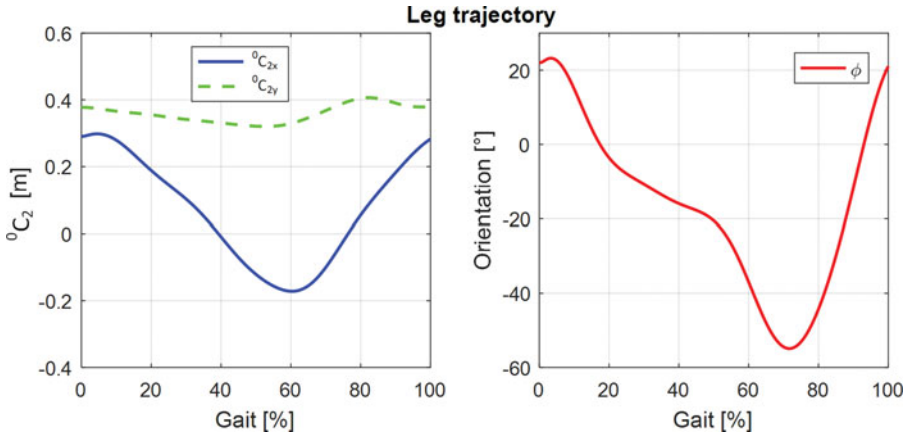

Fig. 7. Leg pose trajectory during a gait cycle for $h = 1.7$ m and tgc $= 0.96$ s.

is shown in Fig. 6. As well as the kinematic model shown in Fig. 2 represents the following: the "upper body" has a prismatic joint with the fixed frame "base" and the body segments ("upper body", "thigh", "leg + orthosis" and "foot") are articulated with three revolute joint blocks: "hip joint", "knee joint" and "ankle joint". Moreover, geometric and inertia specifications are, carefully, written into the body blocks.

Next, the external forces are applied according to the formulation investigated in Section 2. The unloading force "F_{un}" is computed in the block "BWSD" in relation to a desired unloading "BWS" using Eq. (2). Knowing the position of the placement points P_1 and P_2, the footlifter force "F_{lr}" is computed based on the moment equilibrium of the foot weight about the ankle joint. The GRF "R_{gr}" is computed using Eq. (5) and it is applied on the foot segment. Finally, by inputting the curve of the α coefficient (Fig. 4), the action of the upper body force on the thigh is computed inside the block "upper body".

In order to obtain the actuation wrench, the used method is to actuate the lower limb through an active joint "three-DOF planar joint" placed at the leg CoM; however, for the other joints, they are kept passive. This custom joint has two linear and one rotational DOFs taking place in the sagittal plane. The data of the block "lower limb kinematics" (Fig. 5(a)) are fed to the block "leg pose trajectory", in which the leg trajectory (Fig. 7) is computed using equations of the leg pose given in Appendix A.6 and then sent to the leg segment for actuation.

By running the simulation, the actuation wrench ($\mathbf{F}_{\text{cdr}}$, $\mathbf{M}_{\text{cdr}}$) is computed by the solver inside the "three-DOF planar joint" block and this information is collected from the block "actuation wrench ($\mathbf{F}_{\text{cdr}}$, $\mathbf{M}_{\text{cdr}}$)".

It is worth mentioning that the developed model is parameterized, i.e., the parameter values of blocks can be set in the command line. Thereby, all the lengths and inertial specifications of the human body can be easily changed through the script.

5. Cable Tensions

So far, the required wrench is determined using two approaches, the next step is to compute the cable tension capable of producing these forces. To this end, one shall write and solve the end-effector/cables equilibrium problem, shown in Fig. 8. The end effector (orthosis) is controlled by four cables that go out from exit point A_{i} and are connected to the attachment points B_{i}. The location of the points A_{i} and B_{i} are given with respect to reference frames O, x_0, y_0 and C_2, x_2, y_2, respectively. As aforementioned, we assume that the orthosis is fixed relative to the leg, and thus the points B_{i} have known locations with respect to the leg frame. The locations of the cable exit points, the cable interference problem and the non-negative cable tension condition were determined in a previous work by the authors.[14]

The equilibrium of the end effector can be as follows:

$$W\, t = f \tag{7}$$

https://doi.org/10.1017/S0263574718000711 Published online by Cambridge University Press

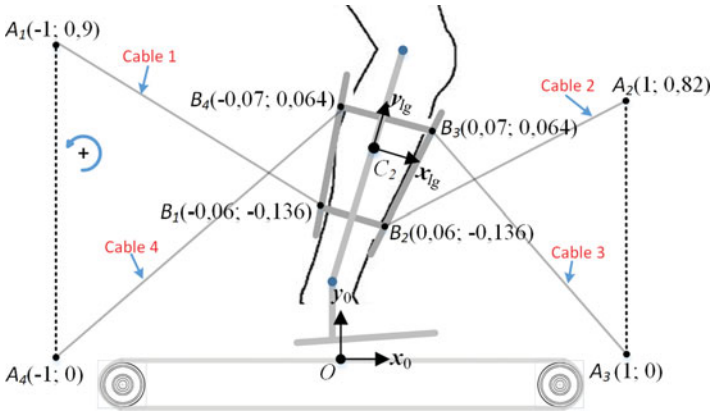

Fig. 8. Specifications of the cable robots.

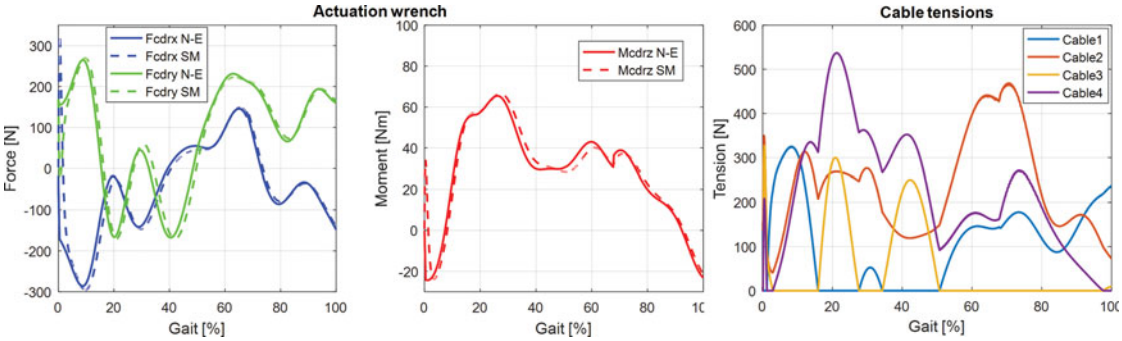

Fig. 9. The actuation wrench (right) and cable tensions (left) during on-ground walking (Newton–Euler (N–E) and Simscape (SM)).

where $W = \begin{pmatrix} d_1 & \cdots & d_4 \\ b_1 \times d_1 & \cdots & b_4 \times d_4 \end{pmatrix}$, $d_i = B_iA_i/\|B_iA_i\|$, $b_i = C_2B_i$, $t = (t_1, ..., t_4)^{\mathrm{T}}$ is the column vector of the cable tensions and $f = (F_{cdrx}, F_{cdry}, M_{cdrz})^{\mathrm{T}}$ is the column vector that represents the external loads (forces and moments). The W matrix is known as the force-moment transformation matrix[25] or the structure matrix[26] and it maps the forces from the cables space to the Cartesian space (loads acting on the robot's effector).

The matrix W is non-square since the robot is redundant; thus, the cable tensions are computed through a linear programming minimization procedure, defined as follows[27]:

$$\min\left(\sum_{i=1}^{4} t_i\right) \quad \text{subject to} \quad W\,t = f \;\&\; t_i \geq 0 \tag{8}$$

The optimization problem (8) minimizes the sum of the cable tensions while ensuring that the equilibrium is achieved and the tensions in the cables are within admissible values. Another possible method is to employ the Moore−Penrose pseudo inverse of redundant manipulators.[28]

6. Results and Discussion

A case study consisting of a body having a weight $m = 100$ kg and a tall $h = 1.7$ m will be used to illustrate the proposed method. Based on anthropometric specifications presented in Fig. 2, all the geometric and inertia data were obtained. Furthermore, the amount of unloading is BWS = 50% and the time of gait cycle is tgc = 0.96 s. Figure 9 shows the plots of the actuation wrench using the two solving approaches, i.e., N–E equations and Simscape model (SM). Results of both approaches are

https://doi.org/10.1017/S0263574718000711 Published online by Cambridge University Press

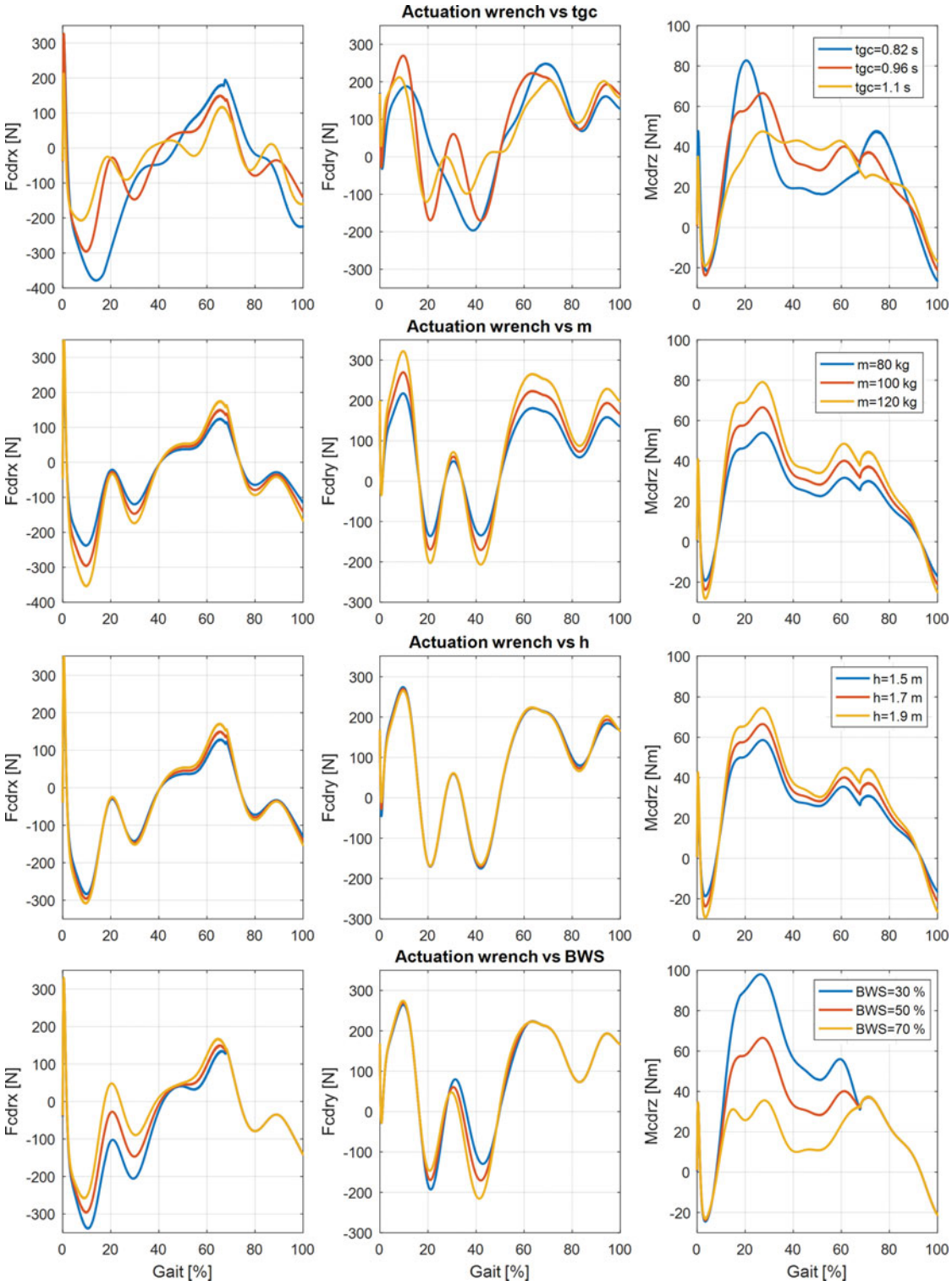

Fig. 10. Actuation wrench in response to the variation of gait training parameters.

consistent, only a small difference can be observed. Besides, using the optimization procedure (8) and the actuation wrench data, the tensions are computed and presented in Fig. 9.

The effect of varying the gait simulation parameters (tgc, m, h and BWS) will be discussed in this section. Figure 10 shows the actuation wrench while the training parameters are varied: time of gait cycle (tgc = 0.82 s, 0.96 s and 1.1 s), body weight (m = 80 kg, 100 kg and 120 kg), body height (h = 1.5 m, 1.7 m and 1.9 m) and unloading percentage (BWS = 30%, 50% and 70%). Note that one

https://doi.org/10.1017/S0263574718000711 Published online by Cambridge University Press

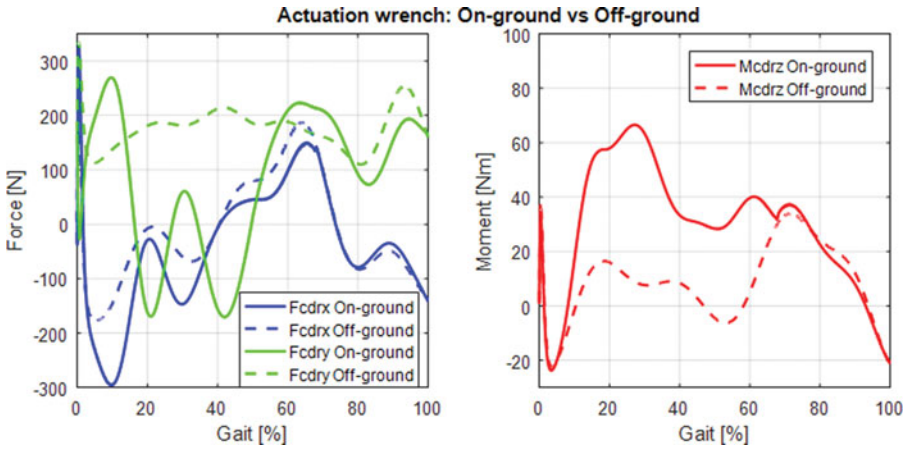

Fig. 11. Actuation wrench for on-ground walking and off-ground walking.

parameter is varied, while the others are kept at their nominal values given as the following: tgc = 0.96 s, $m = 100$ kg, $h = 1.7$ m and BWS = 50%.

Increasing tgc causes the actuation wrenches and the walking speed to increase. The same trend is observed when the body weight m is increased. One can confirm that the mass and the acceleration are determinant factors in the dynamic behavior of the system. Concerning the impact of the body height h, one can notice that $\boldsymbol{F}_{\text{cdrx}}$ increases slightly, $\boldsymbol{F}_{\text{cdry}}$ is practically invariant, and $\boldsymbol{M}_{\text{cdrz}}$ varies slightly in response to an increase in height. An increase in the body weight unloading BWS does not produce any change in $\boldsymbol{F}_{\text{cdry}}$; however, $\boldsymbol{F}_{\text{cdrx}}$ and $\boldsymbol{M}_{\text{cdrz}}$ show a net increase in their values. For the last case, one can observe that the wrench is the same during the swing phase (gait > 68%) since the current lower limb is above the ground; thus, there is no unloading.

The effect of the on-ground/off-ground scenarios is shown in Fig. 11. One can notice that over the swing phase, the on-ground and off-ground curves have almost the same behavior, since in both simulations, the limb is above the ground. The pelvic motion, which is only active for the on-ground case, induces a small difference between the two curves. When comparing both actuation moments $\boldsymbol{M}_{\text{cdrz}}$, it is clear that the required torque is higher for the on-ground walking due to the need to resist the effect of the ground reaction. Conversely, $\boldsymbol{F}_{\text{cdrx}}$ is not sensitive to the ground reaction. In addition, for the off-ground case, the $\boldsymbol{F}_{\text{cdry}}$ component is always positive; therefore, an upward force is required to maintain the leg in the air. Therefore, this force is more influenced by the off-ground walking.

In what follows, the effect of varying the gait training parameters on the cable tensions (Fig. 12) is investigated. The decrease in tgc, i.e., the increase in gait speed, leads to an increase in the tension for cable 2. For the other cables, tensions increase only when tgc goes from 1.1 s to 0.96 s, and a drop is observed for 0.82 s regarding cable 1 and cable 3. Afterwards, when augmenting the mass m, tensions raise gradually for all the cables. Regarding the body height h, its effect is quite small except for cable 2. Furthermore, increasing h leads to a slight increase in the tension of cable 1 and a slight decrease in the tension of cable 3. Finally, due to the absence of unloading during the swing phase, the tensions increase as the unloading BWS decreases, especially for cables 2 and 3. For the on-/off-ground cases, Fig. 13 shows that the tensions are similar during the swing time and throughout the stance period. One can also notice that the required tensions are higher for the on-ground scenario, except for cable 1.

So far, single effects are discussed. Hereafter, the combined effects between gait simulation parameters are investigated with respect to the maximum tension (tm). Previously, we concluded that the effect of the height h is relatively small, compared to the effect of the other three parameters, i.e., tgc, m and BWS. Therefore, the effect of tgc, m and BWS is computed first (Fig. 14) and then that of tgc, m and h (Fig. 15).

Figure 14 shows that higher tgc and lower BWS are major determinants; this result is in agreement with the plot presented in Fig. 13. Considering cables 1 and 4, the maximum tension is obtained for a mass of around 100 Kg. For cables 2 and 3, a monotonic increase in the maximum tension is noticed with the increase in the mass. Figure 15 confirms the previous result, which is the small influence of the

https://doi.org/10.1017/S0263574718000711 Published online by Cambridge University Press

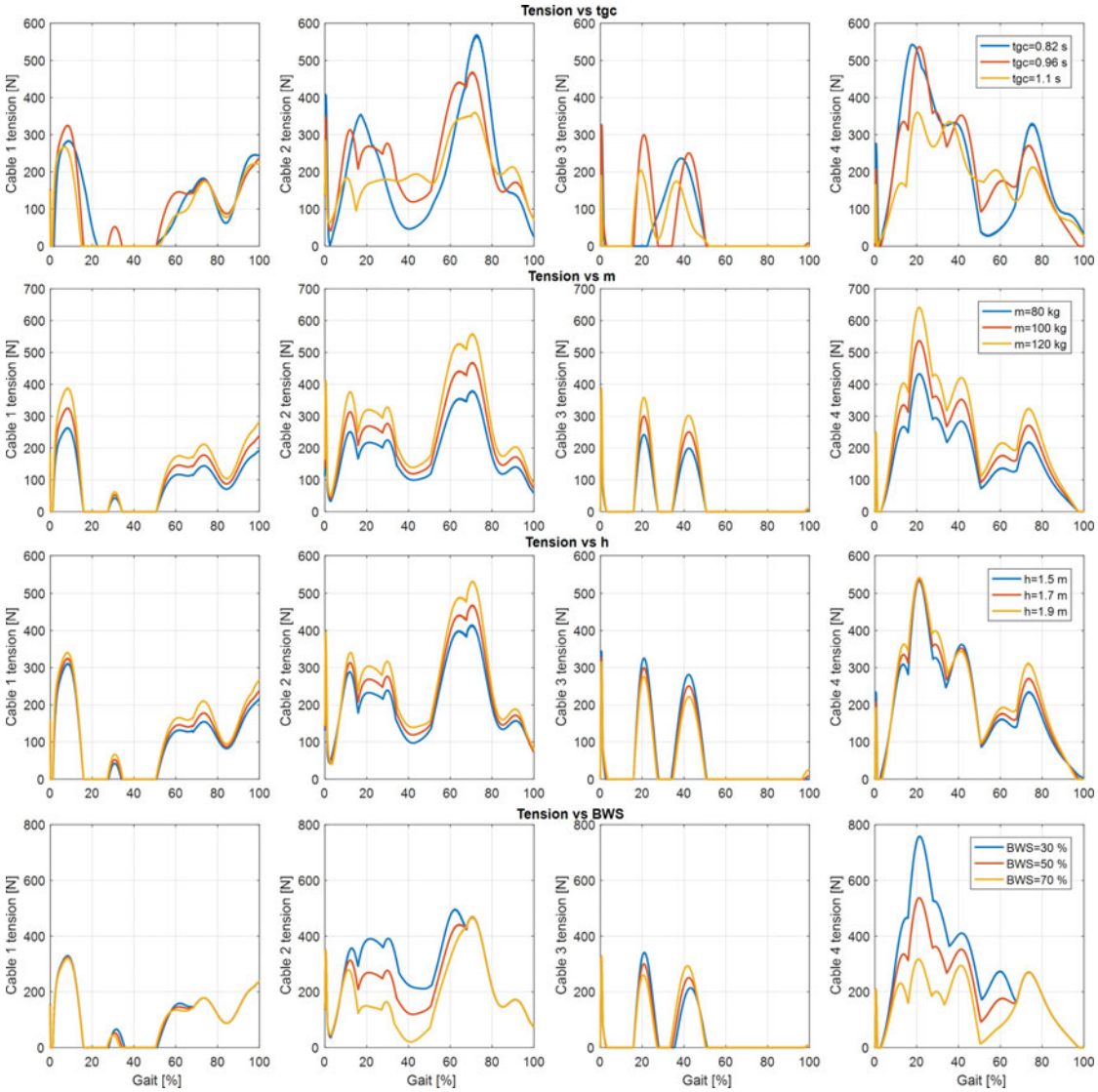

Fig. 12. Cable tensions in response to the variation of gait training parameters.

height on the maximum tensions in the different cables. From a design point of view, the presented results could help the designer in the selection of the CDLT actuators. The scenario of a mass of 100 kg, a height of 1.9 m and an unloading of 70% could be considered as the case requiring the maximum torques from the actuator spooling cable 1.

Moreover, the obtained results are helpful for clinicians in estimating the optimal gait training parameters. Indeed, by means of musculoskeletal models, some effects may be estimated, e.g., the effect of the BWS or the tgc on the muscular activity,[29] and also their effects on a patient with a knee osteoarthritis.[30] Muscle activation is a major indicator to assess the quality of rehabilitation. Commonly, this information is provided using EMGs. In our case, by addressing a muscular model of the lower limb, the joint torques and the muscle forces could be retrieved.

To reach this goal and as a future work, models, addressing the relationship between the muscle activities and the actuation wrenches and the cable tensions, are being developed by the authors.

7. Conclusions

A dynamic simulation and a parametric analysis of an unloaded walking within the CDLT were investigated and described. The target information was the actuation wrench, and consequently, the

https://doi.org/10.1017/S0263574718000711 Published online by Cambridge University Press

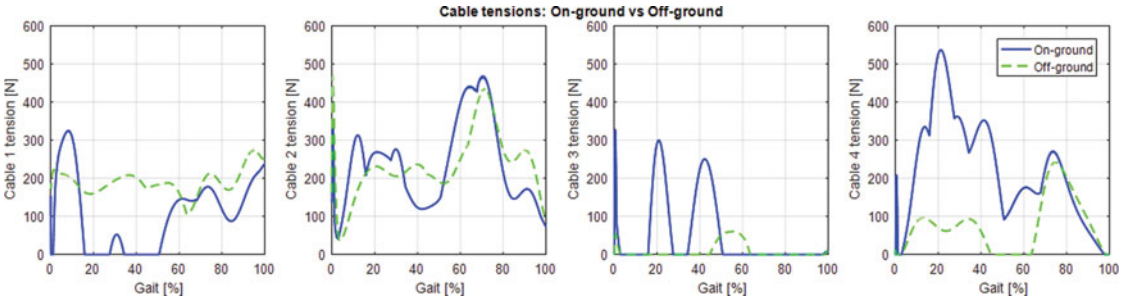

Fig. 13. Cable tensions for on-ground walking and off-ground walking.

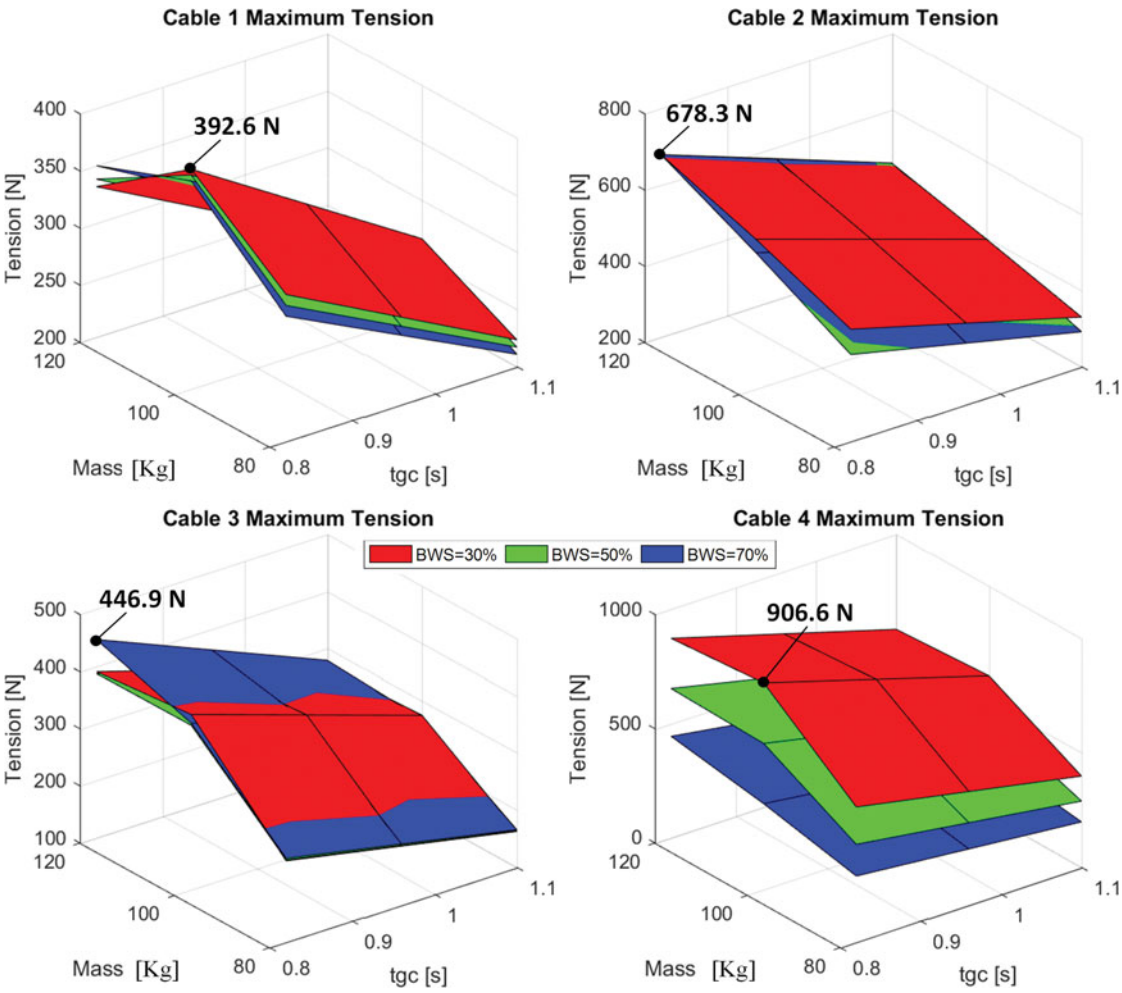

Fig. 14. Maximum tension as a function of tgc, *m* and BWS.

cable tensions required to drive the lower limb. The N–E approach was implemented to solve the dynamic problem. A Matlab Simscape model was also built to validate the analytical results. The gait simulation parameters, i.e., the gait cycle time, the body weight, the patient height and the unloading, were varied in order to observe their effect on the actuation wrench and the cable tensions. Furthermore, combined effects on the maximum tension in the cables were also investigated.

Ongoing works are being carried out to develop musculoskeletal model, which allows the estimation of the activity and contribution of the muscles during the training using the CDLT.

https://doi.org/10.1017/S0263574718000711 Published online by Cambridge University Press

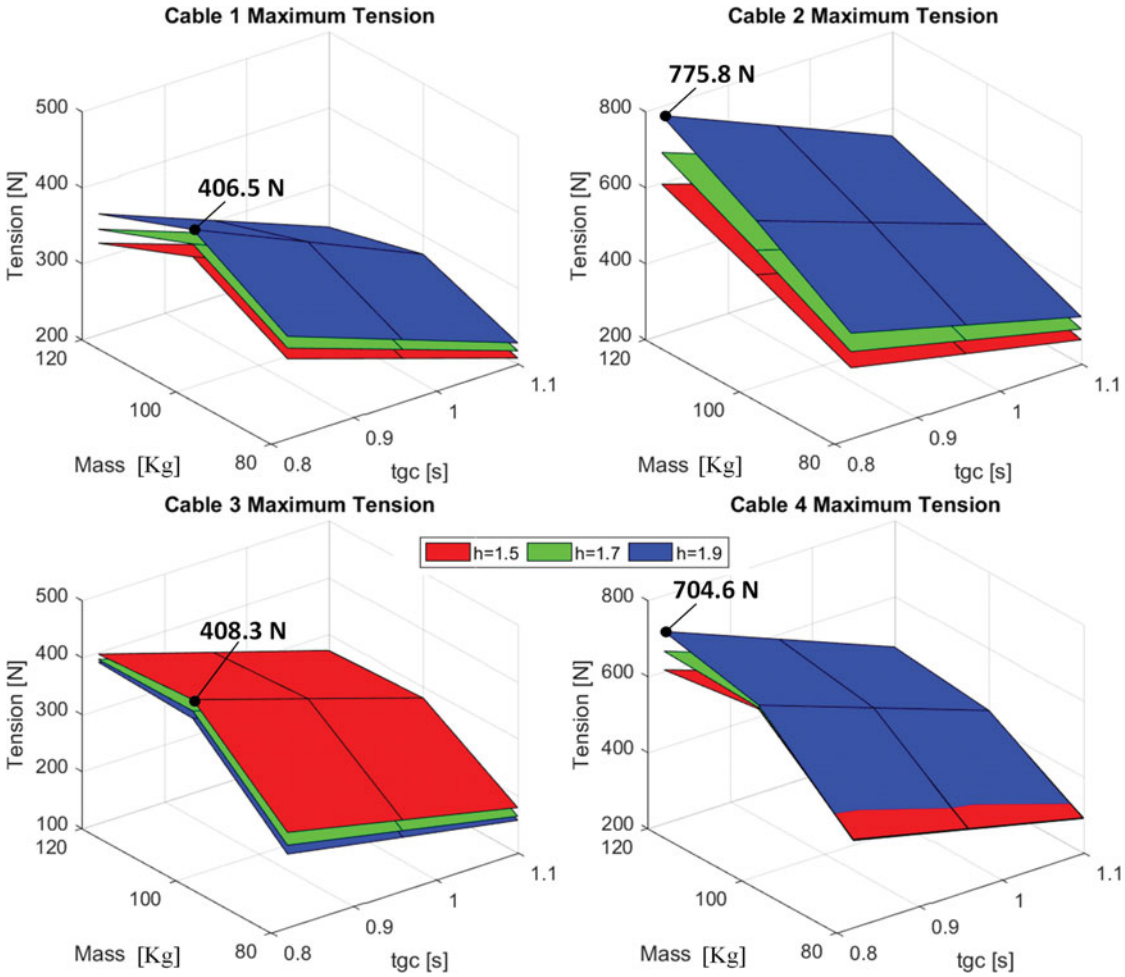

Fig. 15. Maximum tension as a function of tgc, *m* and *h.*

References

1. M. Eltoukhy, J. Oh, C. Kuenze and J. Signorile, "Improved kinect-based spatiotemporal and kinematic treadmill gait assessment," *Gait Posture* **51**, 77–83 (2017).
2. K. Teachasrisaksakul, Z. Zhang, G.-Z. Yang and B. Lo, "Imitation of dynamic walking with BSN for humanoid robot," *IEEE J. Biomed. Heal. Informatics* **19**(3), 794–802 (2015).
3. A. Rajagopal, C. L. Dembia, M. S. DeMers, D. D. Delp, J. L. Hicks and S. L. Delp, "Full-body musculoskeletal model for muscle-driven simulation of human gait," *IEEE Trans. Biomed. Eng.* **63**(10), 2068–2079 (2016).
4. M. S. Shourijeh and J. McPhee, "Foot–ground contact modeling within human gait simulations: From Kelvin–Voigt to hyper-volumetric models," *Multibody Syst. Dyn.* **35**(4), 393–407 (2015).
5. S. L. Delp *et al*., "OpenSim: Open-source software to create and analyze dynamic simulations of movement," *IEEE Trans. Biomed. Eng.* **54**(11), 1940–1950 (2007).
6. D. A. Winter, *Biomechanics and Motor Control of Human Movement*, 4th ed. (John Wiley & Sons, Hoboken, New Jersey, USA, 2009).
7. C. L. Vaughan, B. L. Davis and C. O. Jeremy, *Dynamics of Human Gait*, 2nd ed. (Kiboho Publishers, Cape Town, South Africa, 1999).
8. J. Wojtusch and O. von Stryk, "HuMoD-A Versatile and Open Database for the Investigation, Modeling and Simulation of Human Motion Dynamics on Actuation Level," *Proceedings of the 2015 IEEE-RAS 15th International Conference on Humanoid Robots (Humanoids)* (2015) pp. 74–79.
9. E. J. Dijkstra and E. M. Gutierrez-Farewik, "Computation of ground reaction force using zero moment point," *J. Biomech.* **48**(14), 3776–3781 (2015).
10. S. Springer and G. Yogev Seligmann, "Validity of the kinect for gait assessment: A focused review," *Sensors* **16**(2), 194 (2016).
11. J. L. P. do Rosário, "Biomechanical assessment of human posture: A literature review," *J. Bodyw. Mov. Ther.* **18**(3), 368–373 (2014).

https://doi.org/10.1017/S0263574718000711 Published online by Cambridge University Press

12. E. Dolatabadi, B. Taati and A. Mihailidis, "Concurrent validity of the microsoft kinect for windows v2 for measuring spatiotemporal gait parameters," *Med. Eng. Phys.* **38**(9), 952–958 (2016).
13. F. E. Zajac, R. R. Neptune and S. A. Kautz, "Biomechanics and muscle coordination of human walking: Part I: Introduction to concepts, power transfer, dynamics and simulations," *Gait Posture* **16**(3), 215–232 (2002).
14. H. Lamine, M. Amine Laribi, S. Bennour, L. Romdhane and S. Zeghloul, "Design study of a cable-based gait training machine," *J. Bionic Eng.* **14**(2), 232–244 (2017).
15. J. Benito-Penalva *et al*., "Gait training in human spinal cord injury using electromechanical systems: Effect of device type and patient characteristics," *Arch. Phys. Med. Rehabil.* **93**(3), 404–412 (2012).
16. V. Racic, A. Pavic and J. M. W. Brownjohn, "Experimental identification and analytical modelling of human walking forces: Literature review," *J. Sound Vib.* **326**(1), 1–49 (2009).
17. B. Koopman, H. J. Grootenboer and H. J. De Jongh, "An inverse dynamics model for the analysis, reconstruction and prediction of bipedal walking," *J. Biomech.* **28**(11), 1369–1376 (1995).
18. L. Ren, R. K. Jones and D. Howard, "Whole body inverse dynamics over a complete gait cycle based only on measured kinematics," *J. Biomech.* **41**(12), 2750–2759 (2008).
19. Y. Xiang, J. S. Arora, S. Rahmatalla and K. Abdel-Malek, "Optimization-based dynamic human walking prediction: One step formulation," *Int. J. Numer. Methods Eng.* **79**(6), 667–695 (2009).
20. R. Fluit, M. S. Andersen, S. Kolk, N. Verdonschot and H. F. J. M. Koopman, "Prediction of ground reaction forces and moments during various activities of daily living," *J. Biomech.* **47**(10), 2321–2329 (2014).
21. Y. Jung, M. Jung, J. Ryu, S. Yoon, S.-K. Park and S. Koo, "Dynamically adjustable foot-ground contact model to estimate ground reaction force during walking and running," *Gait Posture* **45**, 62–68 (2016).
22. A. Tözeren, *Human Body Dynamics: Classical Mechanics and Human Movement* (Springer-Verlag New York, New York, USA, 2000).
23. M. Frey, G. Colombo, M. Vaglio, R. Bucher, M. Jorg and R. Riener, "A novel mechatronic body weight support system," *Neural Syst. Rehabil. Eng. IEEE Trans.* **14**(3), 311–321 (2006).
24. J. Hidler, W. Wisman and N. Neckel, "Kinematic trajectories while walking within the Lokomat robotic gait-orthosis," *Clin. Biomech.* **23**(10), 1251–1259 (2008).
25. J. J. Craig, *Introduction to Robotics Mechanics and Control*, 3rd ed. (Pearson Education International, Upper Saddle River, 2005).
26. C. B. Pham, S. H. Yeo, G. Yang and I.-M. Chen, "Workspace analysis of fully restrained cable-driven manipulators," *Rob. Auton. Syst.* **57**(9), 901–912 (2009).
27. H. Lamine, S. Bennour and L. Romdhane, "Design of cable-driven parallel manipulators for a specific workspace using interval analysis," *Adv. Robot.* **30**(9), 585–594 (2016).
28. R. L. Williams and P. Gallina, "Planar cable-direct-driven robots: Design for wrench exertion," *J. Intell. Robot. Syst.* **35**(2), 203–219 (2002).
29. K. Van Kammen, A. Boonstra, H. Reinders-Messelink and R. den Otter, "The combined effects of body weight support and gait speed on gait related muscle activity: A comparison between walking in the Lokomat exoskeleton and regular treadmill walking," *PLoS One* **9**(9), e107323 (2014).
30. S. Watanabe and F. Someya, "Effect of body weight-supported walking on exercise capacity and walking speed in patients with knee osteoarthritis: A randomized controlled trial," *J. Japanese Phys. Ther. Assoc.* **16**(1), 28–35 (2013).

Appendices

A.1. Upper Body Equilibrium

$$F_{\text{uby}} = \alpha \cdot (-(m_{\text{ub}} + m_{\text{oth}}) \cdot g + k((m \cdot g \cdot \text{BWS})/k + \Delta y/2) - (m_{\text{ub}} + m_{\text{oth}}) \cdot a_{\text{uby}})$$

A.2. Thigh Equilibrium

$$F_{\text{thx}} = -(I_{\text{th}}|\dot{\omega}_{\text{thz}} - (C_1H)_x \cdot F_{\text{uby}} + (C_1K)_x \cdot F_{\text{uby}} + (C_1H)_y \cdot a_{\text{thx}} \cdot m_{\text{th}} - (C_1K)_x \cdot a_{\text{thy}} \cdot m_{\text{th}} - (C_1K)_x \cdot g \cdot m_{\text{th}})/((C_1H)_y - (C_1K)_y)$$

$$F_{\text{thy}} = F_{\text{uby}} + a_{\text{thy}} \cdot m_{\text{th}} - g_{\cdot} \cdot m_{\text{th}}$$

A.3. Foot Equilibrium

Stance phase

$$F_{\text{ftx}} = -a_{\text{ftx}} \cdot m_{\text{ft}} - R_{\text{grx}} \cdot (F_{\text{uny}} - g \cdot (m + m_{\text{or}} - m_{\text{lg}} - m_{\text{ft}})m)$$

$$F_{\text{fty}} = -a_{\text{fty}} \cdot m_{\text{ft}} - g \cdot m_{\text{ft}} - R_{\text{gry}} \cdot (F_{\text{uny}} - g \cdot (m + m_{\text{or}} - m_{\text{lg}} - m_{\text{ft}})m)$$

https://doi.org/10.1017/S0263574718000711 Published online by Cambridge University Press

$$F_{\mathrm{lr}} = \|F_{\mathrm{lr}}\| \cdot (P_1P_2/\|P_1P_2\|) \text{ suchthat } \|F_{\mathrm{lr}}\| = 0$$

Swing phase

$$\begin{aligned} F_{\mathrm{ftx}} = (&I_{\mathrm{ft}} \cdot (P_1P_2)_x \cdot \dot{\omega}_{\mathrm{ftz}} + (C_3A)_x \cdot (P_1P_2)_x \cdot a_{\mathrm{fty}} \cdot m_{\mathrm{ft}} - (C_3A)_x \cdot (P_1P_2)_y \cdot a_{\mathrm{ftx}} \cdot m_{\mathrm{ft}} + (C_3P_2)_x \\ &\cdot (P_1P_2)_y \cdot a_{\mathrm{ftx}} \cdot m_{\mathrm{ft}} - (C_3P_2)_y \cdot (P_1P_2)_x \cdot a_{\mathrm{ftx}} \cdot m_{\mathrm{ft}} + (C_3A)_x \cdot (P_1P_2)_x \cdot g \cdot m_{\mathrm{ft}})/(C_3A)_x \cdot (P_1P_2)_y \\ &-(C_3A)_y \cdot (P_1P_2)_x - (C_3P_2)_x \cdot (P_1P_2)_y + (C_3P_2)_y \cdot (P_1P_2)_x) \end{aligned}$$

$$\begin{aligned} F_{\mathrm{fty}} = (&I_{\mathrm{ft}} \cdot (P_1P_2)_y \cdot \dot{\omega}_{\mathrm{ftz}} + (C_3A)_y \cdot (P_1P_2)_x \cdot a_{\mathrm{fty}} \cdot m_{\mathrm{ft}} - (C_3A)_y \cdot (P_1P_2)_y \cdot a_{\mathrm{ftx}} \cdot m_{\mathrm{ft}} + (C_3P_2)_x \\ &\cdot (P_1P_2)_y \cdot a_{\mathrm{fty}} \cdot m_{\mathrm{ft}} - (C_3P_2)_y \cdot (P_1P_2)_x \cdot a_{\mathrm{fty}} \cdot m_{\mathrm{ft}} + (C_3A)_y \cdot (P_1P_2)_x \cdot g \cdot m_{\mathrm{ft}} + (C_3P_2)_x \cdot (P_1P_2)_y \\ &\cdot g \cdot m_{\mathrm{ft}} - (C_3P_2)_y \cdot (P_1P_2)_x \cdot g \cdot m_{\mathrm{ft}})/((C_3A)_x \cdot (P_1P_2)_y - (C_3A)_y \cdot (P_1P_2)_x - (C_3P_2)_x \cdot (P_1P_2)_y \\ &+(C_3P_2)_y \cdot (P_1P_2)_x) \end{aligned}$$

$F_{\mathrm{lr}} = \|F_{\mathrm{lr}}\| \cdot (P_1P_2/\|P_1P_2\|)$ such that

$$\begin{aligned} \|F_{\mathrm{lr}}\| = -(&I_{\mathrm{ft}} \cdot \dot{\omega}_{\mathrm{ftz}} + (C_3A)_x \cdot a_{\mathrm{fty}} \cdot m_{\mathrm{ft}} - (C_3A)_y \cdot a_{\mathrm{ftx}} \cdot m_{\mathrm{ft}} + (C_3A)_x \cdot g \cdot m_{\mathrm{ft}})/((C_3A)_x \cdot (P_1P_2)_y \\ &- (C_3A)_y \cdot (P_1P_2)_x - (C_3P_2)_x \cdot (P_1P_2)_y + (C_3P_2)_y \cdot (P_1P_2)_x) \end{aligned}$$

A.4. Leg Equilibrium

$$\begin{aligned} F_{\mathrm{cdrx}} &= a_{\mathrm{lg}x} \cdot (m_{\mathrm{lg}} + m_{\mathrm{or}}) - F_{\mathrm{lr}x} - F_{\mathrm{th}x} - F_{\mathrm{ftx}} \\ F_{\mathrm{cdry}} &= g \cdot (m_{\mathrm{lg}} + m_{\mathrm{or}}) - F_{\mathrm{lry}} - F_{\mathrm{thy}} - F_{\mathrm{fty}} + a_{\mathrm{lgy}} \cdot (m_{\mathrm{lg}} + m_{\mathrm{or}}) \\ M_{\mathrm{cdrz}} &= \dot{\omega}_{\mathrm{lgz}} \cdot (I_{\mathrm{lg}} + I_{\mathrm{or}}) - (C_2A)_x \cdot F_{\mathrm{fty}} + (C_2A)_y \cdot F_{\mathrm{ftx}} - (C_2P_1)_x \cdot F_{\mathrm{lry}} + (C_2P_1)_y \cdot F_{\mathrm{lrx}} \\ &\quad - (C_2K)_x \cdot F_{\mathrm{thy}} + (C_2K)_y \cdot F_{\mathrm{thx}} \end{aligned}$$

A.5. Thigh Pose

$$\begin{pmatrix} {}^0C_{1x} \\ {}^0C_{1y} \\ \phi_{\mathrm{th}} \end{pmatrix} = \begin{pmatrix} -C_{1y} \cdot \sin(\theta_{\mathrm{hip}}) \\ H_y + C_{1y} \cdot \cos(\theta_{\mathrm{hip}}) \\ \theta_{\mathrm{hip}} \end{pmatrix}$$

A.6. Leg Pose

$$\begin{pmatrix} {}^0C_{2x} \\ {}^0C_{2y} \\ \phi_{\mathrm{lg}} \end{pmatrix} = \begin{pmatrix} C_{2y} \cdot \sin(\theta_{\mathrm{knee}} - \theta_{\mathrm{hip}}) - K_y \cdot \sin(\theta_{\mathrm{hip}}) \\ H_y + K_y \cdot \cos(\theta_{\mathrm{hip}}) + C_{2y} \cdot \cos(\theta_{\mathrm{knee}} - \theta_{\mathrm{hip}}) \\ \theta_{\mathrm{hip}} - \theta_{\mathrm{knee}} \end{pmatrix}$$

A.7. Foot Pose

$$\begin{pmatrix} {}^0C_{3x} \\ {}^0C_{3y} \\ \phi_{\mathrm{ft}} \end{pmatrix} = \begin{pmatrix} C_{3x} \cdot \cos(\theta_{\mathrm{knee}} - \theta_{\mathrm{ankle}} - \theta_{\mathrm{hip}}) + C_{3y} \cdot \sin(\theta_{\mathrm{knee}} - \theta_{\mathrm{ankle}} - \theta_{\mathrm{hip}}) - K_y \cdot \sin(\theta_{\mathrm{hip}}) \\ \quad + A_y \cdot \sin(\theta_{\mathrm{knee}} - \theta_{\mathrm{hip}}) H_y + C_{3y} \cdot \cos(\theta_{\mathrm{knee}} - \theta_{\mathrm{ankle}} - \theta_{\mathrm{hip}}) + K_y \cdot \cos(\theta_{\mathrm{hip}}) \\ \quad - C_{3x} \cdot \sin(\theta_{\mathrm{knee}} - \theta_{\mathrm{ankle}} - \theta_{\mathrm{hip}}) + A_y \cdot \cos(\theta_{\mathrm{knee}} - \theta_{\mathrm{hip}}) \theta_{\mathrm{hip}} - \theta_{\mathrm{knee}} + \theta_{\mathrm{ankle}} \end{pmatrix}$$

https://doi.org/10.1017/S0263574718000711 Published online by Cambridge University Press